

Supplemental Information:

Are MXenes Suitable for Soft Multifunctional Composites?

Cerwyn Chiew¹ and Mohammad H. Malakooti^{1,2,*}

¹*Department of Mechanical Engineering, University of Washington, Seattle, WA 98195, USA*

²*Institute for Nano-Engineered Systems, University of Washington, Seattle, WA 98195, USA*

*Corresponding author: malakoot@uw.edu

1 Eshelby's tensor (Mechanical Property) for finite cylinder and ellipsoidal inclusion

Franciosi et al.^{1,2} derived the Eshelby's tensor for a flat cylinder inclusion by using both volume averaging and radon transform formulation of the elastostatic green's function. This tensor is used to either model stress/strain concentration behavior of monolayer or multilayer MXenes in this study which are embedded in a reference matrix λ which could be either the interphase ($\lambda = i$) or the polymer matrix ($\lambda = m$) of MXPCs.

$$S_\lambda = \left(\begin{array}{ccc|ccc} \frac{3A}{8}\Psi + \psi & \frac{A}{8}\Psi & \frac{A}{2}\beta + \frac{1}{2}\psi & & & \\ \frac{A}{8}\Psi & \frac{3A}{8}\Psi + \phi & \frac{A}{2}\beta + \frac{1}{2}\psi & & 0 & \\ \frac{A}{2}\beta + \frac{1}{2}\psi & \frac{A}{2}\beta + \frac{1}{2}\psi & A\Phi + 2\phi & & & \\ & & & A\psi\phi + (0.5\psi + \phi) & & \\ & & & & A\psi\phi + (0.5\psi + \phi) & \\ & 0 & & & & \frac{A}{4}\Psi \end{array} \right) : C \quad S1$$

$$C = \frac{1}{(1 - 2\nu_\lambda)} \left(\begin{array}{ccc|ccc} (1 - \nu_\lambda) & \nu_\lambda & \nu_\lambda & & & \\ \nu_\lambda & (1 - \nu_\lambda) & \nu_\lambda & & 0 & \\ \nu_\lambda & \nu_\lambda & (1 - \nu_\lambda) & & & \\ & & & 0.5(1 - 2\nu_\lambda) & & \\ & 0 & & & 0.5(1 - 2\nu_\lambda) & \\ & & & & & 0.5(1 - 2\nu_\lambda) \end{array} \right) \quad S2$$

$$A = (1 - \nu_\lambda)^{-1} \quad S3$$

Based on Equation S1 and S2, the 4th order Eshelby's tensor is dependent on the Poisson's ratio (ν_λ) of the reference matrix medium (λ) of the flat cylinder inclusion. This Poisson's ratio could be redefined as the Poisson's ratio of MXene (ν_r), interphase (ν_i), or the polymer phase (ν_m) in IMT model. From radon transformation and volume integral computation, the shape functions (i.e., Ψ, ψ, Φ, β and ϕ) of the finite cylinder Eshelby's tensor are derived and summarized in Equation. S4 to S8. Furthermore, the following shape functions are also dependent on the thickness to diameter ratio (ζ) of the finite cylinder inclusion. In the first homogenization step of the micromechanics IMT model, this ζ is assigned to the reciprocal aspect ratio ($\zeta = \alpha^{-1}$) of monolayer MXene. Alternately, in the second homogenization step of IMT model, ζ becomes the reciprocal aspect ratio of the equivalent medium ($\zeta = \beta^{-1}$). To verify the validity of these shape functions, we ensured that the plotted shape functions in relation to ζ (Figure S1) is identical to those shown in

the original work.² Based on Figure S1, the majority of MXene sheets embedded in MXPCs have size ratio (ζ) that are below 1/500. Hence, when ζ is small, the Eshelby's tensor will represent MXenes as flat cylinder inclusions in the composite.

$$\Psi = \frac{8}{3\pi^2} \left\{ \frac{3}{2} + \frac{3\pi}{4}\zeta - \frac{3+3\zeta^2}{2\zeta} \tan^{-1} \zeta \right\} + \frac{2a_5}{\pi^2} \sqrt{\zeta} \{a_1(I-III) + \alpha\zeta_2(IV-II) + a_3\zeta^2 III - a_4\zeta^3 IV\} \quad S4$$

$$\psi = \frac{8}{3\pi^2} \left\{ 1 + \frac{3\pi}{2}\zeta - \frac{3\zeta^2+1}{\zeta} \tan^{-1} \zeta + \zeta^2 \ln \left(\frac{\zeta^2}{1+\zeta^2} \right) \right\} + 2a_5\pi^{-2} \left(I\zeta^{0.5}(a_1 - a_3\zeta^2) - II\zeta^{\frac{3}{2}}(a_2 - a_4\zeta^2) + 2\zeta^2 \left(c \right. \right. \quad S5$$

$$\Phi = \frac{8}{3\pi^2} \left\{ \frac{5}{2} - \frac{9\pi}{4}\zeta + \frac{1+9\zeta^2}{2\zeta} \tan^{-1} \zeta - 2\zeta^2 \ln \left(\frac{\zeta^2}{1+\zeta^2} \right) \right\} + 1 - \frac{8}{\pi^2} \quad S6$$

$$\phi = \frac{8}{3\pi^2} \left\{ 2 - \frac{3\pi}{2}\zeta + \frac{3\zeta^2+1}{\zeta} \tan^{-1} \zeta - \zeta^2 \ln \left(\frac{\zeta^2}{1+\zeta^2} \right) \right\} + 1 - \frac{8}{\pi^2} \quad S7$$

$$\beta = \frac{8}{3\pi^2} \left\{ -\frac{1}{2} + \frac{3\pi}{4}\zeta + \frac{1-3\zeta^2}{2\zeta} \tan^{-1} \zeta + \zeta^2 \ln \left(\frac{\zeta^2}{1+\zeta^2} \right) \right\} + a_5\pi^{-2} \quad S8$$

In Equation S4 to S8, the coefficient values of a_1 , a_2 , a_3 , a_4 , and a_5 are provided in Table S1. Moreover, the shorthand terms (i.e., I, II, III, and IV) introduced in these equations are also dependent on ζ . These shorthanded terms are all listed from Equation S9 to S12.

$$I = \frac{\sqrt{2}}{2} \left[\pi + \frac{1}{2} \ln \left(\frac{\zeta + \sqrt{2\zeta} + 1}{\zeta - \sqrt{2\zeta} + 1} \right) - \tan^{-1} (1 + \sqrt{2\zeta}) - \tan^{-1} (\sqrt{2\zeta} - 1) \right] \quad S9$$

$$II = \frac{\sqrt{2}}{2} \left(\pi - \frac{1}{2} \ln \left(\frac{\zeta + \sqrt{2\zeta} + 1}{\zeta - \sqrt{2\zeta} + 1} \right) - \tan^{-1} (\sqrt{2\zeta} + 1) - \tan^{-1} (\sqrt{2\zeta} - 1) \right) \quad S10$$

$$III = \frac{\sqrt{2}}{8} \left\{ \pi + \frac{1}{2} \ln \left(\frac{\zeta + \sqrt{2\zeta} + 1}{\zeta - \sqrt{2\zeta} + 1} \right) - \tan^{-1} (\sqrt{2\zeta} + 1) - \tan^{-1} (\sqrt{2\zeta} - 1) + \frac{2\sqrt{2}\zeta\sqrt{\zeta}}{(\zeta^2 + 1)} \right\} \quad S11$$

$$IV = \frac{3\sqrt{2}}{8} \left(\pi - \frac{4\sqrt{\zeta}}{3\sqrt{2}(\zeta^2 + 1)} - \frac{1}{2} \ln \left(\frac{\zeta + \sqrt{2\zeta} + 1}{\zeta - \sqrt{2\zeta} + 1} \right) + \tan^{-1} (1 - \sqrt{2\zeta}) - \tan^{-1} (\sqrt{2\zeta} + 1) \right) \quad S12$$

Table S1: Coefficient values of a_1 to a_5 define the shape function of finite cylinder Eshelby's tensor.

a_1	a_2	a_3	a_4	a_5
$1 + \sqrt{2}/6$	$2 + \sqrt{2}/2$	$1 + \sqrt{2}/2$	$\sqrt{2}/6$	0.729

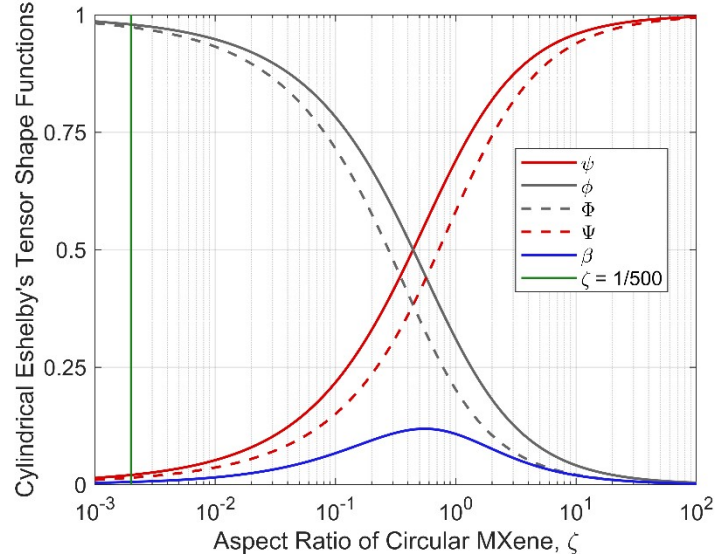


Figure S1. The weight fraction that results from the radon transforms volume integral of circular cylinder for finding the components of Eshelby's tensor. In our study, we will mostly use the weight functions left to the green line which is the majority aspect ratios of our MXene clusters.

2 Flat/finite cylinder Eshelby's tensor (Functional Property)

To model the thermal and dielectric behaviors of MXene polymer composites, the field polarization by MXene inclusions can be evaluated with the help of 2nd order Eshelby's tensor for finite cylinder inclusion.^{1,2} This 2nd order Eshelby's tensor in Equation S13 is used in IMT model to predict the functional properties of MXPCs based on the aspect ratios of embedded single or multilayer MXenes. In the first Mori-Tanaka homogenization step, the following 2nd order Eshelby's tensor is dependent on the aspect ratio of monolayer MXene ($\zeta = \alpha^{-1}$) of the MXene cluster. For the final homogenization step using the interpolated Mori-Tanaka, the same Eshelby's tensor will be used but with the aspect ratio replace with the aspect ratio of the considered MXene cluster ($\zeta = \beta^{-1}$).

$$S_\lambda = \begin{pmatrix} \frac{1}{2}\psi & 0 & \frac{1}{4}\psi \\ 0 & \frac{1}{2}\psi & \frac{1}{4}\psi \\ \frac{1}{4}\psi & \frac{1}{4}\psi & \phi \end{pmatrix} \quad \text{S13}$$

$$S_\Omega^{11} = \frac{1}{2}\psi \quad \text{for } \zeta = \beta^{-1} \quad \text{S14}$$

3 Percolation volume fraction of MXPCs

The first row and column element (i.e., S_Ω^{11}) of Equation S14 and can be used to evaluate the percolation volume fraction (f^*) of MXPCs with randomly oriented single or multilayer MXenes of a prescribed aspect ratio (ζ^{-1}) by using Equation 16. The following relationship between f^* and ζ^{-1} is illustrated in Figure S2. As the diameter to height ratio of multilayer MXene ($\zeta^{-1} = \beta$) increases from 1 to 10^3 , the predicted percolation threshold decreases from 0.33 to approximately close to zero.

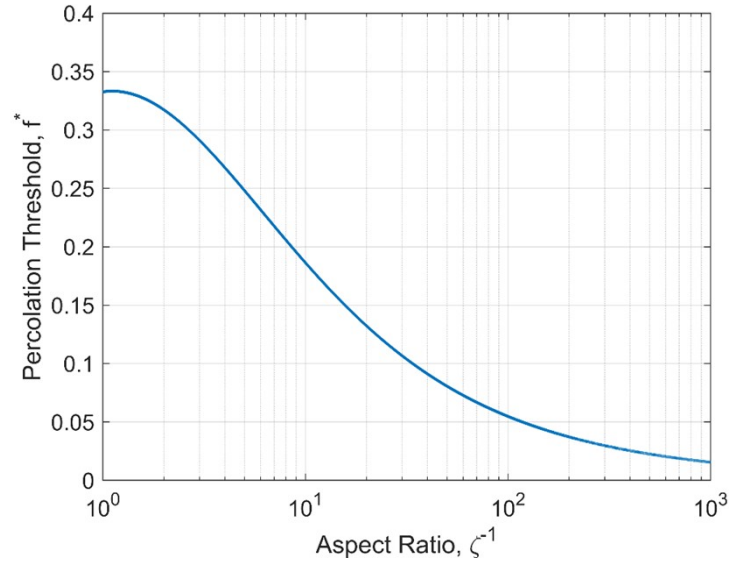


Figure S2. The predicted percolation threshold volume fraction (f^*) as a function of the aspect ratio of multilayer MXenes ($\zeta^{-1} = \beta$).

4 Orientation averaging

When multilayer MXene sheets with high aspect ratios are randomly dispersed in the composite, the effective mechanical and functional properties of the composite will be approximately isotropic. For example, the elastic modulus of the composite in each orthogonal direction (i.e., x, y, and z in Cartesian space) are approximately equivalent to each other. This is because the

orientation of the dispersed MXene inclusions (i.e., flat cylinders) are assumed to be uniformly distributed with respect to each Euler coordinate angles (ϕ , γ , and ψ). To consider random orientation of MXene inclusions in IMT model, the orientation averaging operator (Equation S16) is used.³ Equation S16 is the orientation averaging operator for a given 4th order depolarization tensor (\mathbf{M}) which enables IMT model to compute the effective isotropic mechanical property of MXPCs. The components of this six-by-six matrix (\mathbf{M}) and the orientation averaged matrix $\langle \mathbf{M} \rangle$ are represented as index notation in Equation S17 and S18, respectively. Equation S19 lists the components for the transformation tensor which allows IMT model to account the mechanical reinforcement contributed by individual MXenes embedded at different orientations in the composite.

The property tensor for thermal and dielectric properties of MXPCs are 2nd order tensors. As a result, the orientation averaging operator for IMT model should be compatible for accommodating the orientation averaging of 2nd order tensor (Equation S20). The components of now 3 by 3 depolarization matrix (\mathbf{M}) and the resultant orientation averaged matrix ($\langle \mathbf{M} \rangle$) are listed in Equation S17. Both Equation S17 and S20 are solved using standard rectangular numerical integration established in MATLAB.

$$\langle A \rangle_{klmn} = \frac{1}{2\pi^2} \int_{-\pi}^{\pi} \int_0^{\pi} \int_0^{\frac{\pi}{2}} \Theta_{kp} \Theta_{lq} \Theta_{mr} \Theta_{ns} M_{pqrs} \sin(\gamma) d\phi d\gamma d\psi \quad \text{S15}$$

$$M = \left(\begin{array}{ccccccc} M_{1111} & M_{1122} & M_{1133} & & & & \\ M_{2211} & M_{2222} & M_{2233} & & & & 0 \\ M_{3311} & M_{3322} & M_{3333} & & & & \\ & & & M_{2323} & & & \\ & & & & M_{1313} & & \\ & & & & & M_{1212} & \\ & & & & & & \end{array} \right) \quad \text{S16}$$

$$\langle M \rangle = \left(\begin{array}{ccccccc} \langle M \rangle_{1111} & \langle M \rangle_{1122} & \langle M \rangle_{1133} & & & & \\ \langle M \rangle_{2211} & \langle M \rangle_{2222} & \langle M \rangle_{2233} & & & & 0 \\ \langle M \rangle_{3311} & \langle M \rangle_{3322} & \langle M \rangle_{3333} & & & & \\ & & & 0 & & & \\ & & & & \langle M \rangle_{2323} & & \\ & & & & & \langle M \rangle_{1313} & \\ & & & & & & \langle M \rangle_{1212} \end{array} \right) \quad \text{S17}$$

$$\begin{aligned} \Theta_{11} &= \cos(\phi)\cos(\psi) - \sin(\phi)\cos(\gamma)\sin(\psi) \\ \Theta_{22} &= -\sin(\phi)\sin(\psi) + \cos(\phi)\cos(\gamma)\cos(\psi) \\ \Theta_{33} &= \cos(\gamma) \\ \Theta_{21} &= -\cos(\phi)\sin(\psi) - \sin(\phi)\cos(\gamma)\cos(\psi) \\ \Theta_{23} &= \sin(\gamma)\cos(\psi) \\ \Theta_{31} &= \sin(\phi)\sin(\gamma) \\ \Theta_{32} &= -\cos(\phi)\sin(\gamma) \\ \Theta_{12} &= \sin(\phi)\cos(\psi) + \cos(\phi)\cos(\gamma)\sin(\psi) \end{aligned} \quad \text{S18}$$

$$\langle A \rangle_{ij} = \frac{1}{2\pi^2} \int_{-\pi}^{\pi} \int_0^{\pi} \int_0^{\frac{\pi}{2}} \Theta_{ik} \Theta_{jl} A_{kl} \sin(\gamma) d\phi d\gamma d\psi \quad \text{S19}$$

$$M = \begin{pmatrix} M_{11} & M_{12} & M_{13} \\ M_{21} & M_{22} & M_{23} \\ M_{31} & M_{32} & M_{33} \end{pmatrix} \quad \text{and} \quad \langle A \rangle = \begin{pmatrix} \langle M \rangle_{11} & \langle M \rangle_{12} & \langle M \rangle_{13} \\ \langle M \rangle_{21} & \langle M \rangle_{22} & \langle M \rangle_{23} \\ \langle M \rangle_{31} & \langle M \rangle_{32} & \langle M \rangle_{33} \end{pmatrix} \quad \text{S20}$$

5 Interchangeability of property in IMT model

Table S2 shows that the generalized property tensor (L_λ) of polymer matrix ($\lambda=m$), intercalant ($\lambda=i$), and MXene ($\lambda=\Gamma$) in the interpolated Mori-Tanaka model formulation can be interchanged into stiffness, thermal conductivity, and dielectric tensors.

Table S2. Conversion of general property tensor into mechanical and functional property matrix. $I^{3 \times 3}$ is a three-by-three (2nd order) identity matrix or otherwise (\mathbf{I}) will be a six-by-six identity matrix.

Phase	Mechanical Stiffness	Thermal Conductivity $\mathbf{I} = \frac{K_\lambda}{I^{3 \times 3}}$	Relative Permittivity $\mathbf{I} = \frac{\epsilon_\lambda}{I^{3 \times 3}}$
Polymer ($\lambda=m$)	\mathbf{C}_m	$\frac{K_m}{I^{3 \times 3}}$	$\frac{\epsilon_m}{I^{3 \times 3}}$
Intercalant ($\lambda=i$)	\mathbf{C}_i	$\frac{K_i}{I^{3 \times 3}}$	$\frac{\epsilon_i}{I^{3 \times 3}}$
MXene ($\lambda=\Gamma$)	\mathbf{C}_Γ	$K_\Gamma I^{3 \times 3}$	$\epsilon_\Gamma I^{3 \times 3}$

6 Input material properties for IMT model and finite element method

Table S3. Input mechanical and functional properties of constituents in various MXene composites retrieved from literatures.

Phase	Elastic Modulus (MPa)	Poisson's ratio	Thermal conductivity ($\text{W} \cdot \text{m}^{-1} \cdot \text{K}^{-1}$)	Dielectric Constant (DC)
$\text{Ti}_3\text{C}_2\text{T}_x$ MXene (filler)	9,000 to 70,000 ⁴	0.49	55.8 ⁵	1×10^7
PDMS (Sylgard 184)	1.5 ⁶	0.49	0.27	2.7

7 Comparison of IMT model with density functional theory calculations for thermal conductivity of MXene in epoxy composite.

Table S4. Comparing the thermal conductivity of MXene in epoxy composite predicted by IMT model with those by Wang et al.^[7]. To match the comparison condition, 5 μm diameter monolayer MXene at 1% volume fraction are assumed to be randomly dispersed in the following epoxy composite and the epoxy has chosen thermal conductivity of 0.2 $\text{W} \cdot \text{m}^{-1} \cdot \text{K}^{-1}$.

Type of MXene	MXene's input thermal conductivity ($\text{W}\cdot\text{m}^{-1}\cdot\text{K}^{-1}$) [7]	Our work ($\text{W}\cdot\text{m}^{-1}\cdot\text{K}^{-1}$)	Work of Wang et al. ⁷ ($\text{W}\cdot\text{m}^{-1}\cdot\text{K}^{-1}$)
Ti_3C_2	50.8	0.64	~ 0.5
$\text{Ti}_3\text{C}_2\text{F}_2$	92.94	0.83	~ 0.7
$\text{Ti}_3\text{C}_2\text{O}_2$	140.25	1.01	~ 0.95

8 Resistance Function

Figure S3 shows the resistance function behaviors when the number of layers, lateral size, and volume fraction of MXenes in MXPCs are changed. This plot is created based on Equation 18 where it is assumed that f' is equal to f^* at a given considered aspect ratio ($\zeta^{-1} = \beta$) of multilayer MXene. The following resistance function behaviors represent the change in the interphase property when the volume fraction of MXene fillers increases and is sufficient to form percolation microstructure. As a result, this resistance function will influence the predicted thermal conductivity and dielectric properties of MXene polymer composites when different sizes and layers of MXene fillers are considered.

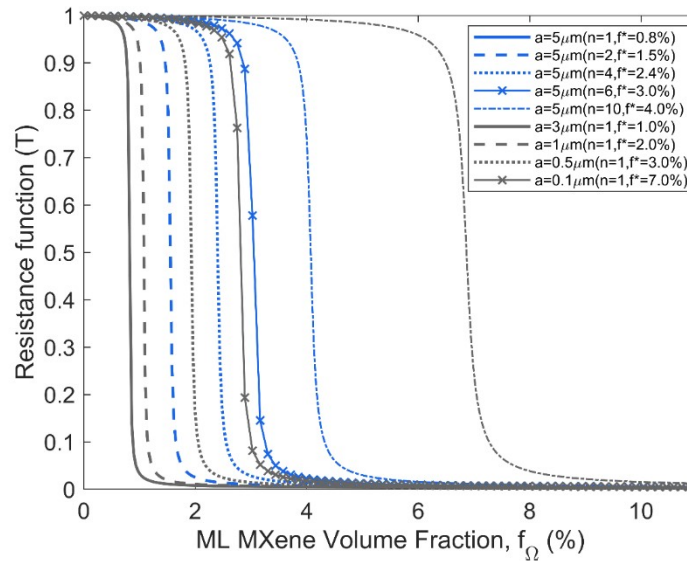


Figure S3. The resistance function as a function of volume fraction due to changes in size (a) and layers (n) of multilayer MXenes. In all this illustrated resistance functions, the resistance decomposition rate (\mathcal{V}_o) is chosen as 0.02.

9 Boundary conditions in FEM

9.1 Mechanical property evaluation

To evaluate the longitudinal Young's modulus of RVE, a uniform normal strain (e_x) is applied on one surface normal to the x-direction ($x=b$) with the opposite surface ($x=0$) set to zero normal displacement (Figure 4). Simultaneously, the surface boundaries of RVE at $y=0$ and $z=0$ will have zero normal displacement while the remainder faces are allowed to freely deform due to Poisson's effect. The obtained reaction force on the fixed surface at $x=0$ is normalized with the surface area of xz plane ($h \cdot b$) to evaluate the applied longitudinal stress (σ_x). By taking the ratio of σ_x and e_x , the longitudinal elastic modulus can be evaluated. To find the transverse (i.e., z-direction) Young's modulus of RVE, a uniform normal strain (e_z) is alternately applied on the surface normal to z-direction ($z=h$) while the opposite surface ($z=0$) is constrained to zero normal displacement. Now, the surface boundaries at $x=0$ and $y=0$ of RVE will have zero normal displacement while other boundaries are left unconstrained. The retrieved reaction force at the constrained surface ($z=0$) normal to applied strain is divided by the surface area of xy plane (b^2) to evaluate the applied transverse stress (σ_z). By taking the ratio of σ_z and e_z , the transverse elastic modulus of the RVE is computed.

9.2 Thermal and dielectric property evaluation

The longitudinal thermal conductivity (κ_p^x) of RVE can be evaluated by applying temperature difference (ΔT) between the surface boundaries at $x=0$ and $x=b$ while other surface boundaries are assumed perfectly insulated (Figure 4b). Then, the total reaction heat flux in x-direction is obtained and normalized with the surface area of xz plane ($h \cdot b$) to recover the heat flux density (q_x) in x-direction. κ_p^x of the representative volume element can be evaluated using the anisotropic Fourier's law in Equation S21. Similarly, the transverse thermal conductivity (κ_p^z) is evaluated by applying temperature gradient (ΔT) between the surface boundaries at $z=0$ and $z=L$ while other surface boundaries to have zero heat flux. Once again, the total reaction heat flux propagating in the z-direction is retrieved and divided by surface area of xy plane (b^2) to derive the heat flux density (q_z). By following Equation S22, the transverse thermal conductivity (κ_p^z) of the RVE is retrieved.

$$\kappa_p^x = q_x \left(\frac{b}{\Delta T} \right) \quad \text{S21}$$

$$\kappa_p^z = q_z \left(\frac{h}{\Delta T} \right) \quad \text{S22}$$

Determining the longitudinal (ϵ_p^x) and transverse (ϵ_p^z) dielectric property is identical to the steps taken for finding the anisotropic thermal conductivity of RVE. The main difference lies in replacing the notion of temperature difference, heat flux, and heat flux density as applied potential field (ΔV), electric flux, and electric flux density. This conversion is possible because the linear constitutive laws of transport properties have similar mathematical form. Hence, the formulae in Equation S21 and S22 can be converted to Equation S23 and S24, respectively. In Equation S23, the electric flux density (D_x) in x-direction needs to be obtained from FEM to evaluate ϵ_p^x . Similarly, in Equation S24, the electric flux density (D_z) in z-direction is retrieved from FEM to find ϵ_p^z .

$$\epsilon_p^x = D_x \left(\frac{b}{\Delta V} \right) \quad \text{S23}$$

$$\epsilon_p^z = D_z \left(\frac{h}{\Delta V} \right) \quad \text{S24}$$

10 Multilayer MXene in hard or soft polymer matrix

Several atomic force microscopy experiments had shown that the measured elastic modulus of $\text{Ti}_3\text{C}_2\text{T}_x$ can range between 9 GPa to 70 GPa while density functional theory simulation had shown that the elastic modulus of $\text{Ti}_3\text{C}_2\text{T}_x$ ranges several hundreds of GPa.⁴ Hence, it is important to investigate if the following range of measured elastic modulus (9 GPa – 70 GPa) of MXenes can influence the effective stiffness of MXPCs.

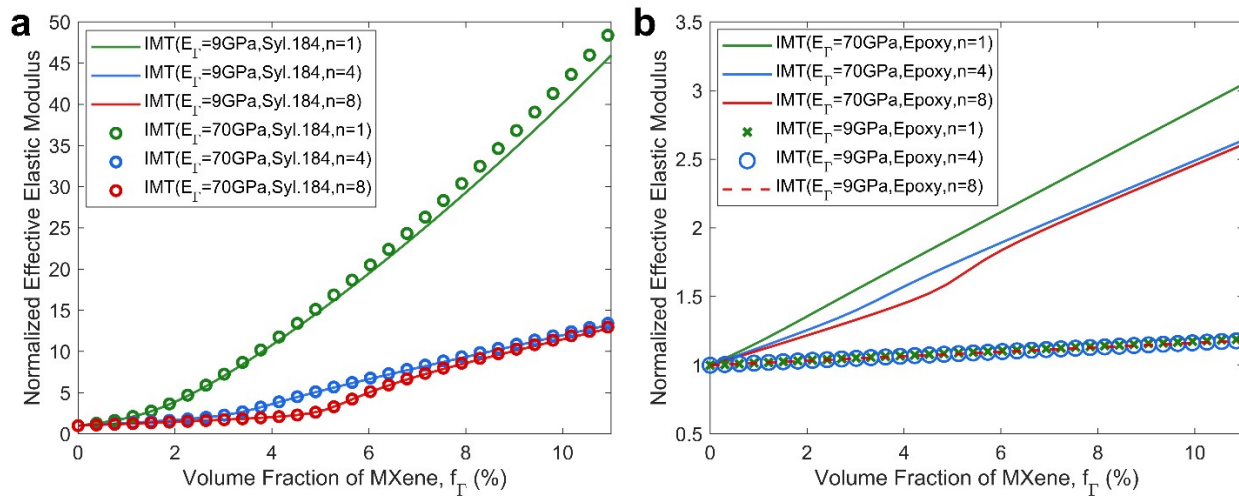


Figure S4. The effects of variation in elastic modulus and multilayer structure of MXene fillers on the predicted elastic modulus of (a) MXene-Sylgard 184 and (b) MXene-Epoxy composite. Both results

assume the size ratio of embedded MXenes are fixed at $\alpha = 500$. Both the predicted elastic modulus of MXPCs in (a) and (b) are respectively normalized by the elastic modulus of unfilled Sylgard 184 and Epoxy polymer.

In Figure S4a, the predicted stiffness of MXene-Sylgard 184 when MXenes' elastic modulus is low (9 GPa) or high (70 GPa) are approximately similar. In addition, this mechanical behavior seems to occur regardless of the number of layers that are considered in the embedded MXenes despite all these fillers having the same lateral size ($a = 500$). On the contrary, IMT model demonstrates that when the considered elastic modulus of MXene is high (70 GPa), the predicted stiffness of MXene in Epoxy composite will be larger than the predicted stiffness of the same Epoxy composite that has low elastic modulus (9 GPa) MXenes (Figure S4b). Hence, this result shows that the predicted elastic modulus of MXene-Epoxy composite is less affected (negligible stiffness suppression effects) by the number of layers present in the embedded MXenes. Based on these comparisons, it can also be concurred that when the polymer matrix of MXPCs is stiff ($E_m \sim 3.5$ GPa) such as epoxy, the stiffness of MXene fillers can more dominantly influence the final elastic modulus of MXPCs rather than the multilayer structure of MXenes. On the other hand, when the elastic modulus ($E_m \sim 1.5$ MPa) of the polymer matrix (Sylgard 184) is low, the effective stiffness of MXPCs becomes more affected by the multilayer structure rather than the stiffness of the MXene fillers.

Reference

1. Franciosi, P., Barboura, S. & Charles, Y. Analytical mean Green operators/Eshelby tensors for patterns of coaxial finite long or flat cylinders in isotropic matrices. *Int J Solids Struct* **66**, 1–19 (2015).
2. Franciosi, P. Mean and axial green and Eshelby tensors for an inclusion with finite cylindrical 3D shape. *Mech Res Commun* **59**, 26–36 (2014).
3. Odegard, G. M., Gates, T. S., Wise, K. E., Park, C. & Siochi, E. J. Constitutive modeling of nanotube–reinforced polymer composites. *Compos Sci Technol* **63**, 1671–1687 (2003).
4. Come, J. *et al.* Nanoscale Elastic Changes in 2D Ti₃C₂T_x (MXene) Pseudocapacitive Electrodes. *Adv Energy Mater* **6**, 1502290 (2016).
5. Liu, R. & Li, W. High-Thermal-Stability and High-Thermal-Conductivity Ti₃C₂T_x MXene/Poly(vinyl alcohol) (PVA) Composites. *ACS Omega* **3**, 2609–2617 (2018).
6. Schneider, F., Fellner, T., Wilde, J. & Wallrabe, U. Mechanical properties of silicones for {MEMS}. *Journal of Micromechanics and Microengineering* **18**, 65008 (2008).
7. Wang, M., Liu, Y., Zhang, H., Wu, Y. & Pan, L. Thermal conductivities of Ti₃C₂T_x MXenes and their interfacial thermal performance in MXene/epoxy composites – a molecular dynamics simulation. *Int J Heat Mass Transf* **194**, 123027 (2022).